SIAM J. Sci. Comput.
Vol. 30, No. 6, pp. 3073–3086

AN ADAPTIVE MULTILEVEL WAVELET SOLVER FOR ELLIPTIC EQUATIONS ON AN OPTIMAL SPHERICAL GEODESIC GRID*

MANI MEHRA† AND NICHOLAS K.-R. KEVLAHAN†

Abstract. An adaptive multilevel wavelet solver for elliptic equations on an optimal spherical geodesic grid is developed. The method is based on second-generation spherical wavelets on almost uniform optimal spherical geodesic grids. It is an extension of the adaptive multilevel wavelet solver [O. V. Vasilyev and N. K.-R. Kevlahan, *J. Comput. Phys.*, 206 (2005), pp. 412–431] to curved manifolds. Wavelet decomposition is used for grid adaption and interpolation. A hierarchical finite difference scheme based on the wavelet multilevel decomposition is used to approximate the Laplace–Beltrami operator. The optimal spherical geodesic grid [*Internat. J. Comput. Geom. Appl.*, 16 (2006), pp. 75–93] is convergent in terms of local mean curvature and has lower truncation error than conventional spherical geodesic grids. The overall computational complexity of the solver is $O(\mathcal{N})$, where $\mathcal{N}$ is the number of grid points after adaptivity. The accuracy and efficiency of the method is demonstrated for the spherical Poisson equation. Although the present paper considers the sphere, the strength of this new method is that it can be extended easily to other curved manifolds by choosing an appropriate coarse approximation and using recursive surface subdivision.

Key words. lifting scheme, second generation wavelets, partial differential equations, optimal spherical geodesic grid, adaptive grid, numerical method, multigrid method

AMS subject classifications. 65M70, 65M55, 35J05

DOI. 10.1137/070689607

1. Introduction. Partial differential equations (PDEs) defined on the sphere and other curved manifolds are common in scientific computation, especially in geophysical fluid dynamics. However, current climate and weather models are not adaptive, which means local features (e.g., hurricanes) are not resolved properly and must be parameterized. The numerical solution of such problems on uniform grids is impractical since high-resolution computations are required only in regions where sharp transitions occur. In particular, there is a need for efficient techniques for the solution of elliptic equations on the sphere (e.g., the Poisson equation for the streamfunction in the quasi-geostrophic equations). In recent years, there has been a growing interest in developing wavelet-based adaptive numerical algorithms for solving elliptic problems [20, 4] and parabolic problems [13, 11, 19, 18, 12]. However, until now these adaptive wavelet methods have been limited to flat geometries (i.e., manifolds with zero curvature).

Efficient and accurate numerical solution of PDEs requires appropriate computational grids. However, on curved manifolds (such as the sphere) the best choice for the computational grid is not obvious. The traditional partition of the sphere is not ideal due to the singularities at the poles which lead to a variety of numerical difficulties, including a severe limitation on the time step unless special measures are undertaken (such as local rescaling of the equations). Because they avoid this problem, quasi-uniform triangulations are gaining popularity in the climate modeling community. Many studies have been made of the development of finite difference and

*Received by the editors April 26, 2007; accepted for publication (in revised form) March 10, 2008; published electronically October 13, 2008. This work was partially supported by NSERC.
http://www.siam.org/journals/sisc/30-6/68960.html

†Department of Mathematics and Statistics, McMaster University, Hamilton, ON, Canada L8S 4K1 (mmehra@math.mcmaster.ca, kevlahan@mcmaster.ca).

finite volume approximation using various spherical triangular grids [10, 23, 14, 7]. Nevertheless, these methods are still nonadaptive.

In a companion paper [16], we developed an adaptive wavelet collocation method for the representation of the Laplace–Beltrami, Jacobian, and flux divergence operators on the sphere. We also demonstrated the accuracy and efficiency of this approach for the adaptive solution of the advection and diffusion equations on the sphere.

The first goal of the present paper is to adapt our approach to use the optimal spherical geodesic grid proposed by Xu [27]. The optimal grid is convergent in the sense of local mean curvature (the standard grid is not convergent) and has lower truncation error for the Laplace–Beltrami operator. Our second goal is to develop an adaptive wavelet multilevel solver for elliptic equations on the sphere using the optimal spherical geodesic grid. We limit ourselves here to the construction of wavelet bases arising from interpolating subdivision schemes. Wavelets are used to adapt the computational grid (and hence compress the solution), while finite differences are used to approximate Laplace–Beltrami operator. The L_2 norm accuracy of both the solution and derivatives are controlled by a tolerance parameter ϵ. This work is an extension of [20] to curved geometries. The elliptic solver can be used for the PDE constraints in evolution problems, such as the Poisson equation in the pressure correction method for the incompressible Navier–Stokes equations. Together, our previous article [16] and the present paper thus provide a complete set of tools for the efficient and accurate adaptive solution of PDEs on the sphere. In particular, we can now solve the full incompressible Navier–Stokes equations on the sphere, taking advantage of wavelet multilevel decomposition and compression. Although we consider the sphere, the strength of this new method is that it can be extended easily to other curved manifolds by choosing an appropriate coarse approximation and using recursive surface subdivision.

The multigrid method is the most efficient method for solving the general systems of algebraic equations obtained from discretizing PDEs. The origin of the multigrid method is found in the papers of Fedorenko [9] and Bakhvalov [1] and in the work of Brandt [2]. The similarities between the multigrid method and the wavelet multiresolution analysis were pointed out by Briggs and Henson [3]. They observed that the space of highest resolution in multiresolution is analogous to the space of fine grid vectors in the multigrid scheme. They also showed that the use of linear interpolation in multigrid schemes corresponds to a representation of the solution in terms of piecewise hat scaling function and that a basis for the null space of the restriction operator spans the wavelet space corresponding to the hat function. In this paper, we exploit the idea of Briggs to develop wavelet-based interpolation (e.g., butterfly interpolation) and restriction operators on an adaptive optimal spherical geodesic grid which is used to construct an adaptive multilevel elliptic solver on the sphere.

The paper is organized as follows. The approximation of the Laplace–Beltrami operator on an optimal spherical geodesic grid and its truncation error compared with the standard spherical geodesic grid are given in section 2. In section 3 an adaptive multilevel wavelet collocation method for solving elliptic PDEs on the optimal grid is described. Finally, section 4 presents the application of the method to the solution of the spherical Poisson equation. The main results are summarized and future directions are outlined in section 5.

2. Approximation of the Laplace–Beltrami operator on an adaptive optimal spherical geodesic grid.

2.1. Wavelets on the sphere. We use the spherical wavelet multiresolution analysis, derivative approximation, and grid adaptation strategy described in [16].

We recall briefly the fundamental ideas underlining the construction of wavelets on the sphere. The interested reader is referred to [16] and [21] for further details.

The construction of spherical wavelets in [21] relies on a recursive partitioning of the sphere into spherical triangles. This is done starting from a platonic solid whose faces are spherical triangles. Successive levels are generated by cutting each triangle into four children. This is accomplished by adding vertices at the midpoint of edges and connecting them with geodetics. Choosing the icosahedron as the starting point, the resulting triangulation has the least imbalance in area between its constituent triangles. Such imbalances, starting from the tetrahedron or octahedron, can lead to visible artifacts. Here we will consider only the icosahedral subdivision for which the number of vertices $\#\mathcal{K}^j = 10 \times 4^j + 2$ at subdivision level j.

Let $\mathcal{S}$ be a triangulation of the sphere S and denote the set of all vertices obtained after subdivisions with $\mathcal{S}^j = \{p_k^j \in S | k \in \mathcal{K}^j\}$, where $\mathcal{K}^j$ is an index set. The vertices of the original platonic solid are in $\mathcal{S}^0$, and $\mathcal{S}^1$ contains those vertices and all new vertices on the edge midpoints. Since $\mathcal{S}^j \subset \mathcal{S}^{j+1}$ we also let $\mathcal{K}^j \subset \mathcal{K}^{j+1}$. Let $\mathcal{M}^j = \mathcal{K}^{j+1}/\mathcal{K}^j$ be the indices of the vertices added when going from level j to $j+1$.

A second generation multiresolution analysis of the sphere provides a sequence of subspaces $\mathcal{V}^j \subset L_2(S)$ with $j \geq 0$ and sphere $S = \{p = (p_x, p_y, p_z) \in \mathbb{R}^3 : \|p\| = a\}$ such that

- $\mathcal{V}^j \subset \mathcal{V}^{j+1}$ (subspaces are nested),
- $\overline{\bigcup_{j\geq 0} \mathcal{V}^j} = L_2(S)$,
- each $\mathcal{V}^j$ has a Riesz basis of scaling functions $\{\phi_k^j | k \in \mathcal{K}^j\}$.

Since $\phi_k^j \in \mathcal{V}^j \subset \mathcal{V}^{j+1}$, for every scaling function ϕ_k^j filter coefficients $h_{k,l}^j$ exist such that

$$\phi_k^j = \sum_{l\in\mathcal{K}^{j+1}} h_{k,l}^j \phi_l^{j+1}. \tag{2.1}$$

Note that the filter coefficients $h_{k,l}^j$ can be different for every $k \in \mathcal{K}^j$ at a given level $j \geq 0$. Therefore each scaling function satisfies a different refinement relation. Each multiresolution analysis is accompanied by a dual multiresolution analysis consisting of nested spaces $\tilde{\mathcal{V}}^j$ with bases given by the dual scaling functions $\tilde{\phi}_k^j$, which are biorthogonal to the scaling functions:

$$\langle \phi_k^j, \tilde{\phi}_{k'}^j \rangle = \delta_{k,k'} \text{ for } k, k' \in \mathcal{K}^j, \tag{2.2}$$

where $\langle f, g\rangle = \int\int_S f g \, \mathrm{d}w$ is the inner product on the sphere. The dual scaling functions satisfy refinement relations with coefficients $\tilde{h}_{k,l}^j$.

A function $u(p) \in L_2(S)$ can be approximated adaptively by filtering the wavelet coefficients d_m^j nonlinearly using a threshold parameter ϵ,

$$u_{\geq}(p) = \sum_{k\in\mathcal{K}^0} c_k^{J_0} \phi_k^{J_0}(p) + \sum_{j=J_0}^{\infty} \sum_{\substack{m\in\mathcal{M}^j \\ |d_m^j|\geq\epsilon}} d_m^j \psi_m^j(p). \tag{2.3}$$

Donoho [6] has shown that for smooth enough u,

$$||u(p) - u_{\geq}(p)||_2 \leq c_1 \epsilon\,. \tag{2.4}$$

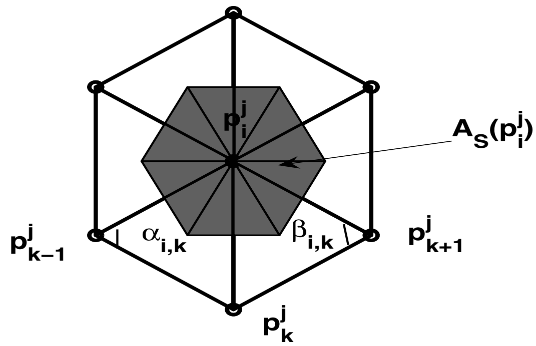

FIG. 1. *The definition of the angles $\alpha_{i,j}$, $\beta_{i,j}$ and neighboring vertices for evaluating the Laplace–Beltrami operator on a spherical triangulation of a surface. Note that these angles include information about the local curvature of the surface.*

Note that removing a wavelet also removes the associated grid point, and so we obtain an approximation to $u(p)$ with L_2 norm accuracy ϵ on an adapted grid. Differential operators are calculated recursively on the adapted grid, starting at the coarsest level. At each level a finite difference approximation using an appropriate weighted sum of neighboring collocation points is used.

When solving PDEs numerically, it is necessary to approximate differential operators of a function from the value of the function at collocation points. We will consider the spherical Poisson equation in the following section. Therefore, we outline the procedure for approximating the Laplace–Beltrami operator on an adaptive optimal spherical geodesic grid in three steps. In sections 2.2 and 2.3, we briefly outline the procedure for numerical approximation of the Laplace–Beltrami operator on a spherical geodesic grid [17] and on an optimal spherical geodesic grid [27], respectively. Finally, in section 2.4 we combine these two ideas to propose the numerical approximation of the Laplace–Beltrami operator on an adaptive optimal spherical geodesic grid.

2.2. Step 1: Calculation of Laplace–Beltrami operator on a spherical geodesic grid. We first review the calculation of the Laplace–Beltrami operator on a standard spherical geodesic grid as described in [16]. For any point p on the surface of S, it is known that [26]

$$\Delta_S p = 2H(p) \in \mathbb{R}^3, \tag{2.5}$$

where $H(p)$ is the mean curvature normal at p, i.e., $\|H(p)\|$ is the mean curvature and $H(p)/\|H(p)\|$ is the unit surface normal. Let p_i^j be a vertex of the triangulation at resolution j and let p_k^j, $k \in N(i)$ be the neighboring vertices around p_i^j. The numerical approximation of the Laplace–Beltrami operator on the sphere $\Delta_{\mathcal{S}}$ as proposed in [17] is then

$$\Delta_{\mathcal{S}} u(p_i^j) = \frac{1}{A_{\mathcal{S}}(p_i^j)} \sum_{k\in N(i)} \frac{\cot\alpha_{i,k} + \cot\beta_{i,k}}{2}[u(p_k^j) - u(p_i^j)], \tag{2.6}$$

where $\alpha_{i,k}$ and $\beta_{i,k}$ are the angles shown in Figure 1 and $N(i)$ is the set of nearest neighbor vertices of the vertex p_i^j. $A_{\mathcal{S}}(p_i^j)$ is the area of the one-ring neighborhood given by

$$A_{\mathcal{S}}(p_i^j) = \frac{1}{8} \sum_{k \in N(i)} (\cot \alpha_{i,k} + \cot \beta_{i,k}) \|p_k^j - p_i^j\|^2. \tag{2.7}$$

Although this construction has been used in practice, it suffers from the fact that the approximation to the local mean curvature of the sphere does not converge. In addition, its truncation error is quite large. We will see that these two faults lead to much larger errors compared with the optimal spherical geodesic grid described in the following section.

2.3. Step 2: Calculation of Laplace–Beltrami operator on an optimal spherical geodesic grid. We start from the spherical geodesic grid described in the previous section. This provides a grid $\mathcal{S}^j$ at level j. The corresponding optimal spherical geodesic grid at level j, denoted as $\mathcal{S}^j_{optm}$, is computed using Algorithm 1 (introduced in [27]).

ALGORITHM 1. OPTIMAL SPHERICAL GEODESIC GRID ($\mathcal{S}^j_{optm}$).
Denote the vertex set $\mathcal{S}^j = \{p_k^{j(0)} \in S | k \in \mathcal{K}^j\}$
do while $\|p_k^{j(l+1)} - p_k^{j(l)}\|_\infty \leq \epsilon_{optm}$
Compute new vertex by $p_k^{j(l+1)} = \frac{1}{A_{\mathcal{S}}(p_i^{j(l)})} \sum_{k \in N(i)} \frac{\cot \alpha_{i,k}^{(l)} + \cot \beta_{i,k}^{(l)}}{4} [p_k^{j(l)} - p_i^{j(l)}]$,
if $v(p_k^{j(l)}) < 6$ ($v(p_k^{j(l)}) \rightarrow$ valence of the vertex $p_k^{j(l)}$)
Project $p_k^{j(l+1)}$ to the unit sphere in the normal direction
end

In Algorithm 1 the norm $\|p_k^{j(l+1)} - p_k^{j(l)}\|_\infty = \max_{k \in \mathcal{K}^j} \|p_k^{j(l+1)} - p_k^{j(l)}\|$. Now we will use the expression (2.6) on $\mathcal{S}^j_{optm}$ to find the Laplace–Beltrami operator on an optimal spherical geodesic grid.

To check the accuracy of the approximation of the Laplace–Beltrami operator on the optimal grid we take the test function

$$u(\theta, \phi) = \sin(\phi), \tag{2.8}$$

where L_∞ and L_2 norms are computed by

$$\|u(p_k^j) - u^j(p_k^j)\|_\infty = \max_{k \in \mathcal{K}^j} (u(p_k^j) - u^j(p_k^j)), \tag{2.9}$$

$$\|u(p_k^j) - u^j(p_k^j)\|_2 = \left[\frac{1}{\sum_{k \in \mathcal{K}^j} \mathcal{A}_{\mathcal{S}}(p_k^j)} \sum_{k \in \mathcal{K}^j} \mathcal{A}_{\mathcal{S}}(p_k^j)(u(p_k^j) - u^j(p_k^j))^2 \right]^{1/2}, \tag{2.10}$$

respectively. Figure 2 shows that the L_∞ norm fails to converge for scales $j > 4$ due to the region around the vertices with valence 5 present in the standard spherical geodesic grid ($\mathcal{S}^j$). However, in the optimal spherical geodesic grid ($\mathcal{S}^j_{optm}$) the error converges in both the norms and with a much smaller truncation error than in the case of the standard grid. This is because $\mathcal{S}^j_{optm}$ is optimal in the sense that the local mean curvature becomes exact around those vertices of valence 5. (There are only 12 such points on the sphere no matter how many scales are used.) In both norms the truncation error is smaller on S^j_{optm} by about a factor of 10. The L_∞ norm has a convergence rate near 1 and the L_2 norm has a slightly better rate. These results are consistent with the linear truncation error estimate given in [27].

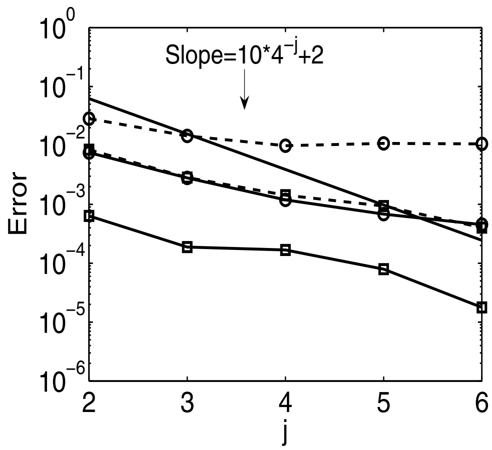

FIG. 2. *Error in Laplace–Beltrami operator as a function of scale* j, $--\circ$ *(*L_∞ *norm on* $\mathcal{S}^j$*),* $-\circ$ *(*L_∞ *norm on* $\mathcal{S}^j_{optm}$*),* $--\square$ *(*L_2 *norm on* $\mathcal{S}^j$*),* $-\square$ *(*L_2 *norm on* $\mathcal{S}^j_{optm}$*),* $-$ *linear convergence of the error.*

2.4. Step 3: Calculation of Laplace–Beltrami operator on an adaptive optimal spherical geodesic grid. A procedure for approximating differential operators, which takes advantage of multiresolution wavelet decomposition, fast wavelet transform, and finite difference differentiation, is discussed in detail by Vasilyev and Bowman [19] for the one-dimensional case and by Vasilyev [18] for multiple dimensions, but is restricted to rectangular domains and flat geometries. The differentiation procedure is based on the interpolating properties of second-generation wavelets. We recall that the wavelet coefficients measure the difference between the approximations of a function at successive levels of resolution j and $j+1$. Thus, if there are no points in the immediate vicinity of a grid point p^j_i, i.e., $|d^j_k| < \epsilon$ for all $k \in N(i)$, and the points p^{j+1}_k, $k \in N(i)$, are not present in $\mathcal{S}^{j+1}_{optm,\geq}$, then there exists some neighborhood of p^j_i, Ω^j_i, where the function can be interpolated by a wavelet interpolant based on $s^j_{k,m}$ $(k \in \mathcal{K}_m)$,

$$\left| u(p) - \sum_{k \in \mathcal{K}_m} s^j_{k,m} \phi^j_k(p) \right| \leq c_3 \epsilon, \tag{2.11}$$

where the coefficients $s^j_{k,m}$ can be chosen according as in [16]. The procedure for finding Laplacian at all grid points is given in Algorithm 2. The wavelets are used to do what they do well: compress and interpolate. Finite differences do the rest: differentiate polynomials. At the end of this procedure we have Laplacian at all grid points with a uniform bound on the approximation error. The computational cost of calculating Laplacian is the same as the cost of forward and inverse transforms.

ALGORITHM 2. APPROXIMATION OF LAPLACE–BELTRAMI OPERATOR ON AN ADAPTIVE OPTIMAL SPHERICAL GEODESIC GRID.

For a function $u(p)$ defined on an adaptive optimal spherical geodesic grid $(\mathcal{S}_{optm,\geq})$,

- Recursively reconstruct the function starting from the coarsest level of resolution. On each level j find Laplacian of the function at grid points that belong to $\mathcal{M}^j_{\geq}$ using the appropriate weighted average (2.6).

The approximation of the Laplace–Beltrami operator on the adapted optimal grid $S_{optm,\geq}$ satisfies the error bound

$$||\Delta_S u(p) - \Delta_S u_{\geq}(p)||_2 \leq c_4\epsilon \leq c_5 N(\epsilon)^{-q}, \tag{2.12}$$

where q is the convergence rate for numerical approximation of the Laplace–Beltrami operator. It also gives us the error bound with $q = 1$ for the numerical solution of the Poisson equation using the adaptive multilevel wavelet solver discussed in the following section.

3. Adaptive multilevel wavelet solver on an optimal spherical geodesic grid. A linear elliptic PDE can be written in the general form

$$\mathcal{L}_S u = f, \tag{3.1}$$

where $\mathcal{L}_S$ is a differential operator on the sphere and f is a source term.

Now, we describe an efficient adaptive multilevel wavelet solver on $\mathcal{S}_{optm,\geq}$ for determining u to within a specified residual tolerance which is an extension of adaptive multilevel solver in [20] from flat geometries. The scheme for the multilevel elliptic solver on an optimal spherical geodesic grid is presented in Algorithm 3, a graphical representation of the scheme for the local multilevel elliptic solver is presented in Figure 3, and a more compact recursive definition of the local multilevel elliptic solver is given in Algorithm 4, where J_0 is the coarsest level of resolution and e^{J_0} is the solution of the residual equation at the coarsest level. The symbol $u_{\geq,j} \leftarrow (\mathcal{L}_S, f^j, u_{\geq,j}, \nu)$ means to relax the algebraic system $\mathcal{L}_s u_{\geq,j} = f^j$ ν times. The integers ν_1 and ν_2 are smoothing parameters in the scheme that control the number of relaxation sweeps before and after the coarse grid. $\mathcal{I}^j_{j-1}$ is the interpolation operator (based on the butterfly interpolation presented in [16] and [21]) which takes coarse grid vectors at level $(j-1)$ and returns fine grid vectors at level j. $\mathcal{I}^{j-1}_j$ is a restriction (injection) operator which moves a vector from a fine grid at level j to coarse grid at level $(j-1)$. An application of this algorithm is presented in the following section.

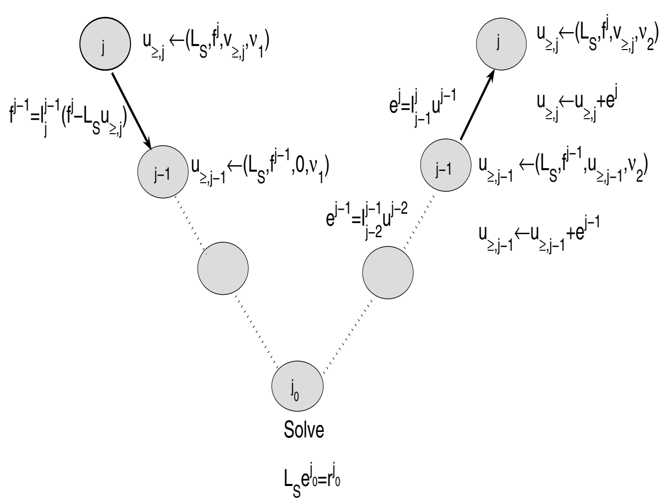

FIG. 3. *Graphical representation of the local multilevel elliptic solver using V-cycles.*

Algorithm 3. Adaptive multilevel wavelet solver on an optimal spherical geodesic grid.

Choose parameters:

- A coarsest level J_0.
- A threshold parameter $\epsilon > 0$.
- Positive adjacent zone constants M and L.

Iterative grid adaptation:

m = 0

$\mathcal{S}_{optm,\geq,m} = \mathcal{S}^{J_0}_{optm}$

do while $m = 0$ or $\mathcal{S}_{optm,\geq,m} \neq \mathcal{S}_{optm,\geq,m-1}$ or $||u_{\geq,m} - u_{\geq,m-1}||_\infty > \delta$

Sample function $u(p)$ on $\mathcal{S}_{optm,\geq,m}$ to give $u_{\geq,m}$.

m = m+1

Forward wavelet transform

Compression: retain only significant coefficients $|d^j_k| \geq \epsilon$ to initialize $\mathcal{S}_{optm,\geq,m}$.

Reconstruction check: (described in [19])

add grid points needed to calculate significant coefficients.

add all points at coarsest level: $\mathcal{S}^{J_0} \subset \mathcal{S}_{optm,\geq,m}$.

Adaptation: add grid points associated with adjacent zone (described in [16, 19]).

Inverse wavelet transform: interpolates $u_{\geq,m}$ onto new grid $\mathcal{S}_{optm,\geq,m}$.

do while $\|f - \mathcal{L}_\mathcal{S} u_{\geq,m}\|_\infty > \delta$

Local multilevel elliptic solver: V–cycle(f^m, $u_{\geq,m}$, m), (**Algorithm** 4)

end

end

Converged results: $\mathcal{S}_{optm,\geq} = \mathcal{S}_{optm,\geq,m}$, $u_\geq = u_{\geq,m}$.

In Algorithm 3 the procedure for grid refinement starts from the coarse grid. Once the solution is obtained, the computational grid consists of the significant grid points and those grid points that could become significant during the next iteration. In other words, at any instant of time the computational grid consists of the $N(\epsilon)$ significant grid points plus those grid points in an adjacent zone in both position and scale that could become significant in the next iteration [13]. We say that the wavelet $\psi^{j'}_l(p)$ belongs to the adjacent zone of wavelet $\psi^j_k(p)$ if the following relations are satisfied:

$$|j - j'| \leq L, \quad |2^{j'-j}k - l| \leq M, \tag{3.2}$$

where L determines the extent to which coarser and finer scales are included in the adjacent zone. This allows for the development of details on finer scales such as shocks or eddies. The parameter M defines the width of the adjacent zone at the same level.

Algorithm 4. Local multilevel elliptic solver using V-cycles.

V-cycle(f^j, $v_{\geq,j}$, j)

Relax ν_1 times on $\mathcal{L}_\mathcal{S} u_{\geq,j} = f^j$ with initial guess $v_{\geq,j}$

if ($j == J_0$)

goto **label:**

else

$f^{j-1} \leftarrow \mathcal{I}^{j-1}_j (f^j - \mathcal{L}_\mathcal{S} v_{\geq,j})$

$v_{\geq,j-1} \leftarrow 0$

$v_{\geq,j-1} \leftarrow$ **V-cycle**(f^{j-1}, $v_{\geq,j-1}$, $j-1$)

end

Correct: $v_{\geq,j} \leftarrow v_{\geq,j} + \mathcal{I}^j_{j-1} v_{\geq,j-1}$, goto **label:**

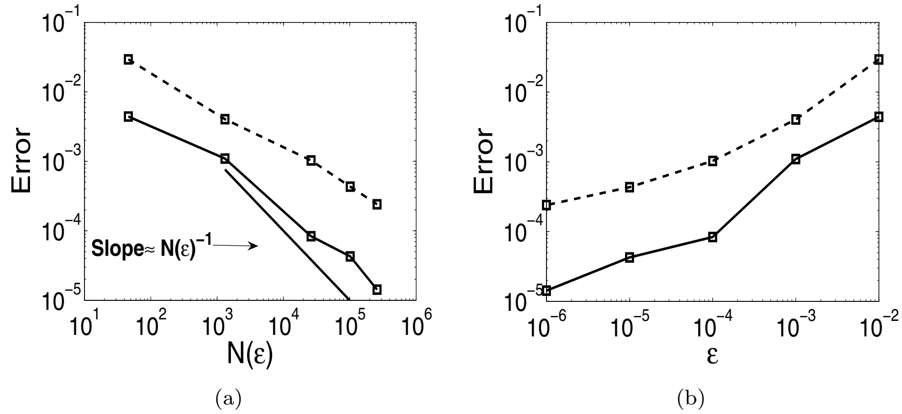

FIG. 4. *Convergence results for the first test case* (a) *as a function of $N(\epsilon)$, and* (b) *as a function of ϵ $--\square$ (L_2 norm on $\mathcal{S}_{\geq}$), $-\square$ (L_2 norm on $\mathcal{S}_{optm,\geq}$).*

label:
Relax ν_2 times on $\mathcal{L}_{\mathcal{S}} u_{\geq,j} = f^j$ with initial guess $v_{\geq,j}$

4. Results and discussion. To illustrate the accuracy and efficiency of the proposed numerical method, we will take the Poisson equation ($\mathcal{L}_S = \Delta_S$) with two different analytical solutions. For the first test case, we take the following analytical solution:

$$u(\theta, \phi) = \sin(\phi). \tag{4.1}$$

Next, we study the convergence of the adaptive multilevel wavelet solver with respect to ϵ using the butterfly wavelet with lifting. Equation (2.4) predicts that decreasing ϵ reduces the error proportionally (by increasing the number of significant grid points $N(\epsilon)$). Hence, the approximation of the solver is controlled by ϵ, d, and q.

In Figure 4(a) the error is presented for different numbers of significant grid points $N(\epsilon)$. This result also verifies the analytical error estimate (2.12). The analytical error estimate (2.4) for the solution is verified in Figure 4(b). Both figures show the much lower error associated with the optimal grid $\mathcal{S}_{optm,\geq}$ compared with the standard grid $\mathcal{S}_{\geq}$. Using the multilevel solver on the adaptive optimal grid $\mathcal{S}_{optm,\geq}$, we achieve the same numerical accuracy as on the adaptive nonoptimal grid $\mathcal{S}_{\geq}$ but with many fewer significant grid points. The adaptive multilevel solver on $\mathcal{S}_{optm,\geq}$ also shows faster convergence compared to the adaptive multilevel solver on $\mathcal{S}_{\geq}$ (as demonstrated in Figure 4).

The increase in the number of grid points and the maximum level of resolution j with the number of global iteration (m) of Algorithm 3 are shown, respectively, in Figures 5(a) and 5(b) for $\epsilon = 10^{-4}$. These results show that the solution is obtained on a near optimal grid: the adaptive multilevel wavelet collocation method uses the minimal number of grid points necessary to obtain the specified error $O(\epsilon)$.

To demonstrate the efficiency of the adaptive algorithm we need to compare the number of grid points used in the adaptive and nonadaptive methods. This may be measured by compression coefficient $\mathcal{C} = N(\epsilon = 0)/N(\epsilon)$. The larger the compression rate, the more efficient the adaptive algorithm. A compression rate of one indicates that there is no compression (i.e., the grid is nonadaptive). Figure 6 shows that the

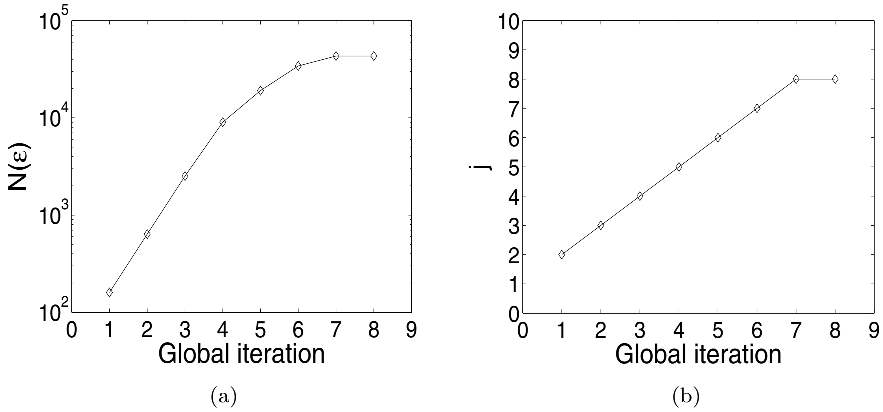

FIG. 5. *Number of global iteration* (*m*) *(threshold* $\epsilon = 10^{-4}$*):* (a) *as a function of the number of significant grid points* $N(\epsilon)$*, and* (b) *as a function of the maximum level of resolution* j*.*

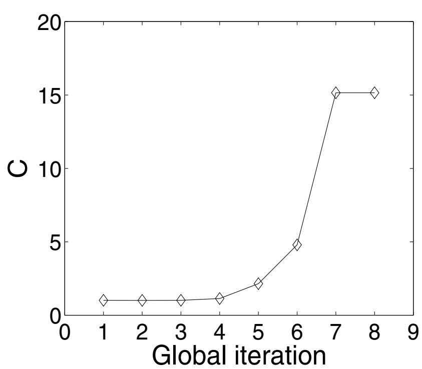

FIG. 6. *The compression coefficient* $\mathcal{C}$ *as a function of global iteration number (m) for threshold* $\epsilon = 10^{-4}$.

compression rate converges rapidly to about 16, which is reasonably high for this very smooth test problem.

In Figure 7 we show how the error converges with respect to global iteration number m in the L_∞ and L_2 norms for $\epsilon = 10^{-4}$. These results show that each V-cycle reduces the error by a fixed proportion, as expected for a multigrid type method. Note that the L_∞ norm gives an artificially large error due to the 12 valence 5 points where the local mean curvature does not converge. Since the number of such points is fixed on the optimal grid (independent of maximum resolution j), the error measured in the L_2 norm converges as expected as $j \to \infty$.

The overall efficiency of the method depends on the convergence of local multilevel elliptic solver (Algorithm 4). Figure 8 shows the residual error up to the discretization error in both norms as a function of the number of local iterations for different smoothing parameters ν_1 and ν_2. We observe from Figure 8 that doubling the relaxation parameter gives the same level of residual error in half the number of V-cycles.

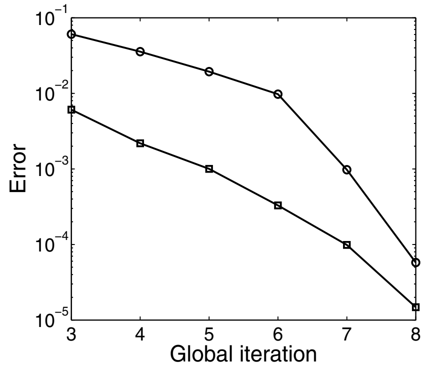

FIG. 7. *Convergence results for the first test case as a function of global iteration* (m), $-\circ$ *(*L_∞ *norm on* $\mathcal{S}_{optm,\geq}$*),* $-\Box$ *(*L_2 *norm on* $\mathcal{S}_{optm,\geq}$*).*

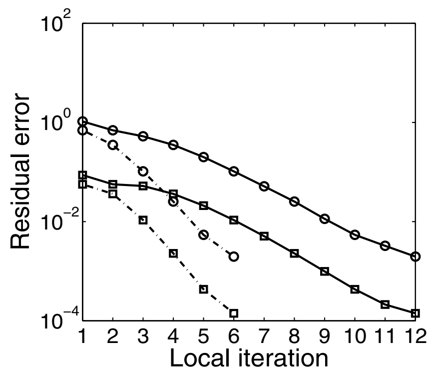

FIG. 8. *Residual error as a function of local iteration number for threshold* $\epsilon = 10^{-4}$ *and different choice of smoothing parameters* ν_1 *and* ν_2*,* $-\circ$ *(*L_∞ *norm,* $\nu_1 = \nu_2 = 2$*),* $-\cdot\circ$ *(*L_∞ *norm,* $\nu_1 = \nu_2 = 4$*),* $-\Box$ *(*L_2 *norm,* $\nu_1 = \nu_2 = 2$*),* $-\cdot\Box$ *(*L_2 *norm,* $\nu_1 = \nu_2 = 4$*).*

Next, we consider a second test case with the following localized analytical solution:

$$u(\theta, \phi) = \exp\left[-\frac{(\theta-\theta_0)^2 + (\phi-\phi_0)^2}{\nu}\right], \tag{4.2}$$

where $\nu = 1/4\pi^2$, $\theta_0 = 0$, and $\phi_0 = 0$. Since this solution is more strongly localized than the first test problem, adaptivity will be even more important for an efficient solution.

To get a better idea of how the adaptive algorithm follows the region of sharp transition, we have plotted the solution using the adaptive multilevel wavelet solver and the corresponding adaptive optimal spherical geodesic grid of solution in Figure 9 with respect to a different global iteration (m). The adaptive optimal spherical geodesic grid converges at level of resolution $j = 9$ and global iteration $m = 8$. This indicates that the localized structure has been resolved within the specified tolerance ϵ. Moreover, in this case we find a compression coefficient $\mathcal{C} \approx 80$ which shows that the number of grid points in adaptive optimal spherical geodesic grid $(\mathcal{S}_{optm,\geq})$ is approximately 80 times less than on a similar nonadaptive optimal spherical geodesic

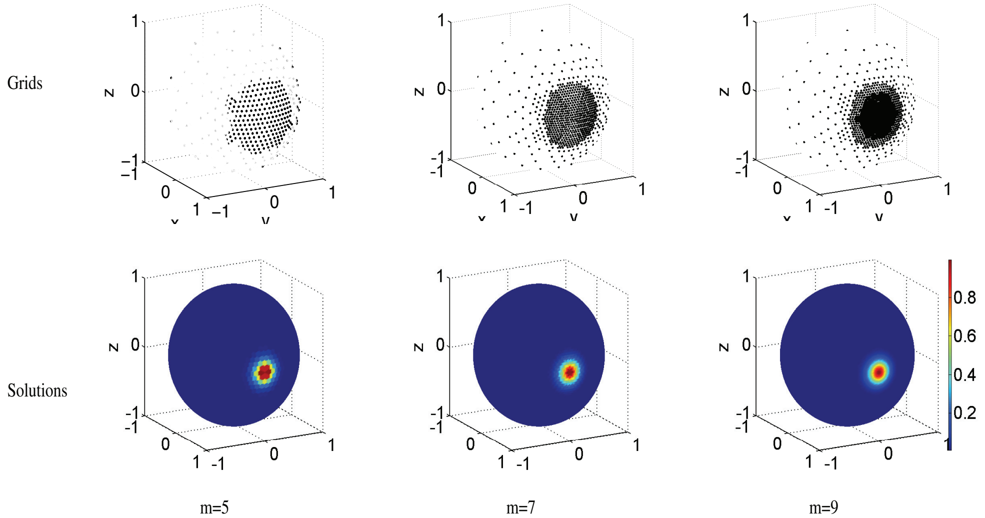

Fig. 9. *Adaptive optimal spherical geodesic grids and corresponding solution of second test case for different* m *with* $\epsilon = 10^{-4}$.

grid ($\mathcal{S}^j_{optm}$ for a fixed j). We have thus demonstrated that our method can accurately and efficiently solve highly localized elliptic PDEs on the sphere. For more comparisons between adaptive and nonadaptive methods, see [16].

We have implemented the adaptive multilevel solver in C++ using the tree data structure explained in [21]. Since this tree data structure is adaptive, our adaptive wavelet method uses less memory as well as less CPU time compared to a nonadaptive elliptic solver.

5. Summary and future work. We have described an adaptive multilevel wavelet solver for elliptic equations on an optimal spherical geodesic grid. Wavelet decomposition is used for grid adaption and interpolation, while an $O(\mathcal{N})$ hierarchical finite difference scheme based on the wavelet multilevel decomposition is used to approximate the Laplace–Beltrami operator on an adaptive optimal spherical geodesic grid. The optimal spherical geodesic grid (proposed by [27]) ensures convergence of the local mean curvature and a lower truncation error. The improved truncation error and efficiency of the solver on an optimal spherical geodesic grid is demonstrated using the Poisson equation.

Our results show that the computational grid adapts efficiently to the local gradients of the solution, refining or coarsening as necessary to achieve the specified error tolerance. This error control is done automatically by specifying one parameter at the beginning of the simulation: the wavelet filtering parameter ϵ. Furthermore, the solution is obtained on a near optimal grid: the adaptive multilevel solver uses the minimal number of grid points necessary to obtain the specified error $O(\epsilon)$.

We studied the compression of model atmospheric turbulence data by spherical wavelets in our previous work [16] and found that approximately half the modes are required to achieve 10^{-2} accuracy in wavelet reconstruction and 1% of the modes qualitatively capture the energy spectrum at all scales. With the elliptic solver described here, we now have all the tools needed to construct fully adaptive solvers for a wide variety of geophysical fluid dynamics problems (e.g., two-dimensional turbulence, quasi-geostrophic, shallow water equations). We intend to use our adaptive wavelet solver to perform large-scale geophysical simulations of atmosphere and ocean dynamics problems.

To tackle earth-scale problems in geophysical fluid dynamics we need a very efficient numerical implementation of our method. We already use a tree data structure (to use memory efficiently). The next step is to parallelize the wavelet transform using `mpi` to take advantage of processing power of the large parallel machines now available. We expect parallelization to be relatively straightforward given the multiscale structure of the wavelet transform.

Acknowledgment. This work was made possible by the facilities of the Shared Hierarchical Academic Research Computing Network (SHARCNET).

REFERENCES

[1] N. S. Bakhvalov, *On the convergence of a relaxation method with natural constraints on the elliptic operators*, USSR Comput. Math. Phys., 6 (1966), pp. 101–135.
[2] A. Brandt, *A multilevel adaptive solutions of boundary value problems*, Math. Comput., 31 (1977), pp. 333–390.
[3] W. L. Briggs and V. E. Henson, *Wavelets and multigrid*, SIAM J. Sci. Comput., 14 (1993), pp. 506–510.
[4] A. Cohen, W. Dahmen, and R. DeVore, *Adaptive wavelet methods for elliptic operator equations: Convergence rates*, Math. Comput., 70 (2001), pp. 27–75.
[5] R. A. Devore, B. Jawerth, and B. J. Lucier, *Image compression through wavelet transform coding*, IEEE Trans. Info. Theory, 38 (1992), pp. 719–746.
[6] D. L. Donoho, *Interpolating Wavelet Transforms*, Technical report 408, 1992.
[7] Q. Du, M. D. Gunzburger, and L. Ju, *Voronoi-based finite volume methods, optimal Voronoi meshes, and PDEs on the sphere*, Comput. Method. Appl. Mech. Engrg., 192 (2003), pp. 3933–3957.
[8] N. Dyn, D. Levin, and J. Gregory, *A butterfly subdivision scheme for surface interpolation with tension control*, ACM Trans. Graphics, 9 (1990), pp. 160–169.
[9] R. P. Fedorenko, *A relaxation method for solving elliptic difference equations*, USSR Comput. Math. Phys., 1 (1962), pp. 1092–1096.
[10] R. Heikes and D. A. Randall, *Numerical integration of the shallow-water equations on a twisted icosahedral grid. Part* I*: Basic design and results of tests*, Mon. Wea. Rev., 123 (1995), pp. 1862–1880.
[11] M. Holmstrom and J. Walden, *Adaptive wavelet methods for hyperbolic PDE's*, J. Comput. Phys., 13 (1998), pp. 19–49.
[12] N. K.-R. Kevlahan and O. V. Vasilyev, *An adaptive wavelet collocation method for fluid-structure interaction at high Reynolds numbers*, SIAM J. Sci. Comput., 26 (2005), pp. 1894–1915.
[13] J. Liandrat and P. Tchamitchian, *Resolution of the* 1*d Regularized Burgers Equation Using a Spatial Wavelet Approximation*, Technical report, NASA Contractor Report 187480, ICASE Report 90-83, NASA Langley Research Center, Hampton, VA 1990.
[14] D. Majewski, D. Liermann, P. Prohl, B. Ritter, M. Buchhold, T. Hanish, G. Paul, and W. Wergen, *The operational icosahedral-hexagonal gridpoint model GME: Description and high-resolution tests*, Mon. Wea. Rev., 130 (2002), pp. 319–338.
[15] U. F. Mayer, *Numerical Solutions for the surface Diffusion Flow in Three Space Dimensions*, Comput. Appl. Math., 20 (2001), pp. 361–379.
[16] M. Mehra and N. K.-R. Kevlahan, *An adaptive wavelet collocation method for the solution of partial differential equations on the sphere*, J. Comput. Phys., 227 (2008), pp. 5610–5632.
[17] M. Meyer, M. Desbrun, P. Schroder, and A. Barr, *Discrete differential-geometry operators for triangulated* 2*-manifolds*, in Visualization and Mathematics, Math. Vis., Springer-Verlag, Berlin, 2003, pp. 35–57.
[18] O. V. Vasilyev, *Solving multi-dimensional evolution problems with localized structure using second generation wavelets*, Int. J. Comput. Fluid Dyn., 17 (2003), pp. 151–168.
[19] O. V. Vasilyev and C. Bowman, *Second generation wavelet collocation method for the solution of partial differential equations*, J. Comput. Phys., 165 (2000), pp. 660–693.

[20] O. V. Vasilyev and N. K.-R. Kevlahan, *An adaptive multilevel wavelet collocation method for elliptic problems*, J. Comput. Phys., 206 (2005), pp. 412–431.
[21] P. Schröder and W. Sweldens, *Spherical wavelets: Efficiently representing functions on the sphere*, in Proceedings of SIGGRAPH (Los Angeles, 1995), ACM, New York, 1995, pp. 161–172.
[22] G. Simonett, *The Willmore flow for near spheres*, Differential Integral Equations, 14 (2001), pp. 1005–1014.
[23] G. R. Stuhne and W. R. Peltier, *New icosahedral grid-point discretization of the shallow water equation on the sphere*, J. Comput. Phys., 148 (1999), pp. 23–58.
[24] W. Sweldens, *The lifting scheme: A construction of second generation wavelets*, SIAM J. Math. Anal., 29 (1998), pp. 511–546.
[25] D. L. Williamson, J. B. Drake, J. J. Hack, R. Jacob, and P. N. Swarztrauber, *A standard test set for numerical approximations to the shallow water equations in spherical geometry*, J. Comput. Phys., 102 (1992), pp. 211–224.
[26] T. J. Willmore, *Riemannian Geometry*, Clarendon Press, Oxford, UK, 1993.
[27] G. Xu, *Discrete Laplace-Beltrami operator on sphere and optimal spherical triangulation*, Internat. J. Comput. Geom. Appl., 16 (2006), pp. 75–93.